Ultrafast Dynamics in Postcollision Interaction after Multiple Auger Decays in Argon 1*s* Photoionization

R. Guillemin,[1,2] S. Sheinerman,[3] C. Bomme,[1,2] L. Journel,[1,2] T. Marin,[1,2] T. Marchenko,[1,2] R. K. Kushawaha,[1,2] N. Trcera,[4] M. N. Piancastelli,[1,2,*] and M. Simon[1,2]

[1]*UPMC, Université Paris 06, LCPMR, 11 Rue Pierre et Marie Curie, 75231 Paris Cedex 05, France*
[2]*CNRS, LCPMR (UMR7614), 11 Rue Pierre et Marie Curie, 75231 Paris Cedex 05, France*
[3]*Department of Physics, St. Petersburg State Maritime Technical University, 198262 St. Petersburg, Russia*
[4]*Synchrotron SOLEIL, l'Orme des Merisiers, Saint-Aubin, BP 48, 91192 Gif-sur-Yvette Cedex, France*

(Received 19 March 2012; published 2 July 2012)

Argon 1*s* photoionization followed by multiple Auger decays is investigated both experimentally, by means of photoelectron-ion coincidences, and theoretically. A strong influence of the different Auger decays on the photoelectron spectra is observed through postcollision interaction which shifts the maximum of the energy distribution and distorts the spectral shape. A good agreement between the calculated and measured spectra for selected Ar^{n+} ions ($n = 1$–5) allows one to estimate the widths (lifetimes) of the intermediate states for each specific decay pathway.

DOI: 10.1103/PhysRevLett.109.013001 PACS numbers: 32.80.Aa, 31.15.xg, 32.70.Jz, 32.80.Fb

The natural lifetime of excited electronic states determines the time scale on which processes following the photoexcitation of a system, an atom, or a molecule will take place. Core-level photoexcitation brings this time scale down to the femtosecond, as core-hole lifetimes are typically a few femtoseconds for shallow core levels in the soft x-ray region and 1 fs or less for deep core levels, and thus provides an internal clock that allows the study of ultrafast phenomena. The understanding of ultrafast processes is critical and has motivated a wealth of studies [1] as these processes are a driving force behind phenomena that extend from radiation damage to the control of chemical reactions at the molecular level. One possible way to look at the dynamics of photoemission is to study the effects of postcollision interaction (PCI) on the line shape of the photoelectron peak. Photoionization of deep atomic shells, $1s^2$ of argon in this study, can be followed by a number of Auger decays which lead to the formation of multiply charged ionic states. Auger decay can lead to the emission of one [single Auger decay (SA)], two [double Auger decay (DA)], or several electrons [multiple Auger decay (MA)] from intermediate or valence shells. In turn, emission of a few electrons can occur simultaneously (direct Auger decay) or sequentially, through the creation and decay of an intermediate quasistationary state (cascade Auger decay). Auger emission by means of SA, DA, or MA processes changes the charge state of the ion which affects strongly the motion of the emitted photoelectron by means of PCI. In the cascade process, a series of subsequent nonradiative relaxations leaves the atom in different core excited states, each with a different lifetime, depending on the decay pathways. The nascent photoelectron thus "feels" an ionic charge that changes with time as the cascade unfolds. In general, PCI takes into account the response of the photoelectron to the variation of the ionic field during the Auger decay, and the interaction between the photoelectron and Auger electrons. Therefore, the dynamical change in the Coulomb potential felt by the photoelectron on a femtosecond scale can be revealed by the analysis of the photoelectron line shapes in terms of PCI.

PCI effects have been well investigated both experimentally and theoretically in SA processes [2,3]. The recent development of experimental techniques, particularly multielectron-coincidence spectroscopy (MECS) [4,5], allows one to investigate the emission of two or more electrons in inner-vacancy decays. Measurements [6] and theoretical models [7–10] show strong PCI distortion of the photoelectron spectra associated with DA processes. PCI in cascade MA processes with emission of three or more electrons has been much less documented [7,11,12], and these investigations concern mainly the PCI influence on threshold photoelectrons. One can expect strong PCI distortions of low-energy-photoelectron spectra associated with cascade MA processes following deep-shell ionization. The effectiveness of MECS is limited in this case by the large energy difference between slow photoelectrons (typically less than 10 eV) and fast Auger electrons (hundreds or thousands of eV). To our knowledge, the more effective method presented in this article, which is based on coincidences between a slow photoelectron and a selected ion, has never been used before to investigate PCI in multiple Auger decay. Our present investigation reveals a strong distortion of the line shape depending on the final charge state and on the lifetime of the intermediate states. Calculations of the photoelectron line shapes for ionic charge up to +5, which take into account PCI effects in SA, DA, and MA processes are presented. The good agreement found between the measured and calculated spectra shows the reliability of the method, and allows us to

estimate the widths (or lifetimes) of the quasistationary intermediate ionic states involved in the Auger decays.

The measurements were performed using synchrotron radiation on beam line LUCIA [13] at SOLEIL, France. The photon energy was calibrated on the argon $1s \rightarrow 4p$ resonance at 3203.54 eV and ionization threshold (IP) at 3206.26 eV [14]. The data were collected using a double-momentum spectrometer [15]. In our experimental geometry, the photon beam crosses a cold supersonic jet of argon at a right angle, forming an interaction volume of approximately $0.1 \times 1 \times 2$ mm^3. Electrons and ions are separated, and accelerated towards two time-of-flight spectrometers positioned perpendicularly to the photon beam and atomic jet, with a static electric field (typically 20 V/cm) chosen to collect within a 4π solid angle all the photoelectrons and ions with a maximum kinetic energy of 8 eV. The particles are detected with 80 mm position-sensitive detectors using delay lines [16]. Both time of flight and impact positions of the ions and electrons detected in coincidence were recorded, allowing us to measure the (Vx, Vy, Vz) components of the initial velocity vectors $\mathbf{V}_{n^+}$ and $\mathbf{V}_{e^-}$ for each (Ar^{n+}, e^-) coincident event between a selected Ar^{n+} ion and a photoelectron e^-. The kinetic energy of the photoelectron is then derived from its velocity vector.

The different Auger processes following Ar $1s$ photoionization were studied in detail previously [11,14,15,17,18], and it is not the aim of this article to discuss the different decay pathways. Although several decay channels can lead to the same final ionic charge, we consider here only the main decay channels contributing to the creation of each Ar^{n+} ion that were clearly identified. These main channels are summarized in Fig. 1, and detailed below.

Ar^+ is created by the direct photoionization of a $1s$ electron, and the core hole decays through $K\beta$ photon emission, leaving the ion singly charged,

$$\gamma + \mathrm{Ar} \rightarrow e_{\mathrm{ph}} + \mathrm{Ar}^{+*}(1s^{-1}) \rightarrow e_{\mathrm{ph}} + \gamma_1 + \mathrm{Ar}^+(3p^{-1}). \quad (1)$$

Ar^{2+} ionic states are reached in two steps: first, $K\alpha$ radiative decay of the $1s$ to a $2p$ vacancy, followed by SA decay of the $2p$ hole:

$$\begin{aligned}\gamma + \mathrm{Ar} &\rightarrow e_{\mathrm{ph}} + \mathrm{Ar}^{+*}(1s^{-1}) \\ &\rightarrow e_{\mathrm{ph}} + \gamma_1 + \mathrm{Ar}^{+*}(2p^{-1}) \\ &\rightarrow e_{\mathrm{ph}} + \gamma_1 + e_{A1} + \mathrm{Ar}^{2+}(3p^{-2}). \end{aligned} \quad (2)$$

Ar^{3+} ions are obtained by a cascade DA which occurs through creation and decay of the intermediate $(2p^{-1}3p^{-1})$ state,

$$\begin{aligned}\gamma + \mathrm{Ar} &\rightarrow e_{\mathrm{ph}} + \mathrm{Ar}^{+*}(1s^{-1}) \\ &\rightarrow e_{\mathrm{ph}} + e_{A1} + \mathrm{Ar}^{2+*}(2p^{-1}3p^{-1}) \\ &\rightarrow e_{\mathrm{ph}} + e_{A1} + e_{A2} + A^{3+}(3p^{-3}). \end{aligned} \quad (3)$$

To reach the Ar^{4+} ionic states, the $1s$ vacancy decays by cascade Auger decay in the first step of which an Auger electron is emitted and the intermediate two-hole $(2p^{-2})$ state is created. The second step is a direct DA decay of this state with emission of two Auger electrons,

$$\begin{aligned}\gamma + \mathrm{Ar} &\rightarrow e_{\mathrm{ph}} + \mathrm{Ar}^{+*}(1s^{-1}) \\ &\rightarrow e_{\mathrm{ph}} + e_{A1} + \mathrm{Ar}^{2+*}(2p^{-2}) \\ &\rightarrow e_{\mathrm{ph}} + e_{A1} + e_{A2} + e_{A3} + A^{4+}(3p^{-4}). \end{aligned} \quad (4)$$

Ar^{5+} ions are obtained after cascade Auger decay occurs through creation and decay of an intermediate two-hole $(2s^{-1}2p^{-1})$ state. $(2p^{-1})$ decays by SA, and $(2s^{-1})$ decays by cascade DA through the intermediate $(2p^{-1})$ state,

$$\begin{aligned}\gamma + \mathrm{Ar} &\rightarrow e_{\mathrm{ph}} + \mathrm{Ar}^{+*}(1s^{-1}) \\ &\rightarrow e_{\mathrm{ph}} + e_{A1} + \mathrm{Ar}^{2+*}(2s^{-1}2p^{-1}) \\ &\rightarrow e_{\mathrm{ph}} + e_{A1} + e_{A2} + e_{A3} + \mathrm{Ar}^{4+*}(2p^{-1}3p^{-3}) \\ &\rightarrow e_{\mathrm{ph}} + e_{A1} + e_{A2} + e_{A3} + e_{A4} + A^{5+}(3p^{-5}). \end{aligned} \quad (5)$$

The experimental and theoretical photoelectron spectra are shown in Figs. 2 and 3 for 2 eV ($h\nu = 3208.3$ eV) and

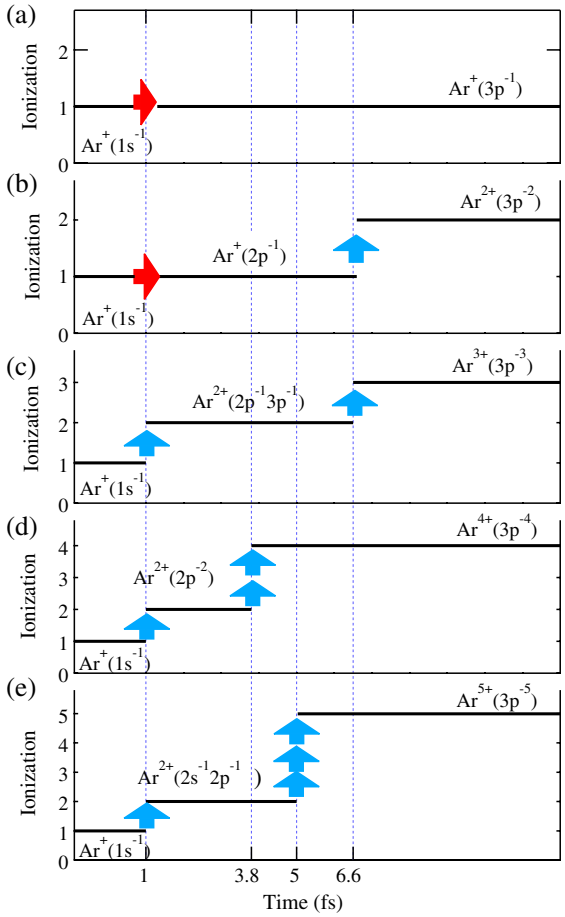

FIG. 1 (color online). Decay pathways leading to the production of Ar^{n+}, with $n = 1$–5, as assumed in our model. The horizontal arrows in panel (a) and (b) represent $K\beta$ and $K\alpha$ radiative decays, respectively. Vertical arrows represent Auger decays. Estimated lifetimes are given in the text.

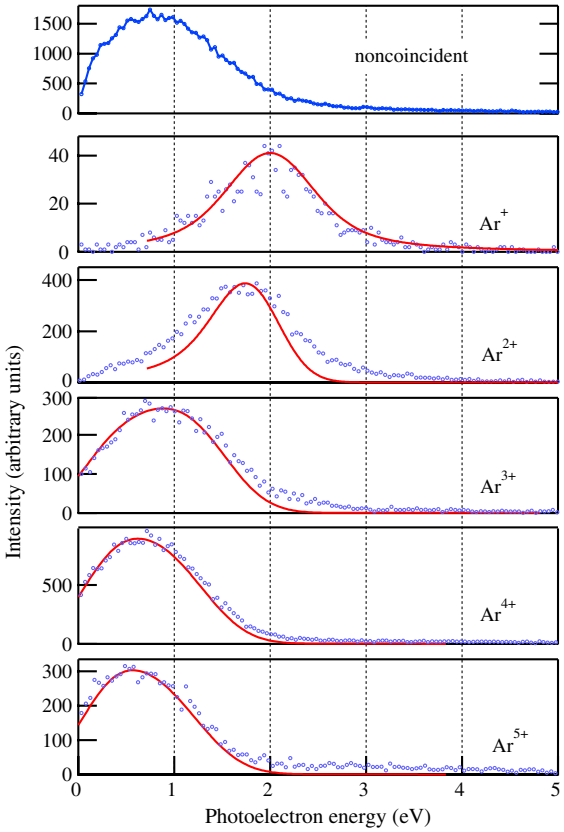

FIG. 2 (color online). Experimental (circles) and theoretical (solid) partial photoelectron spectra measured in coincidence with Ar^{n+} ions ($n = 1$–5) for excess energy 2 eV above IP. The top curve shows the noncoincident photoelectron spectrum.

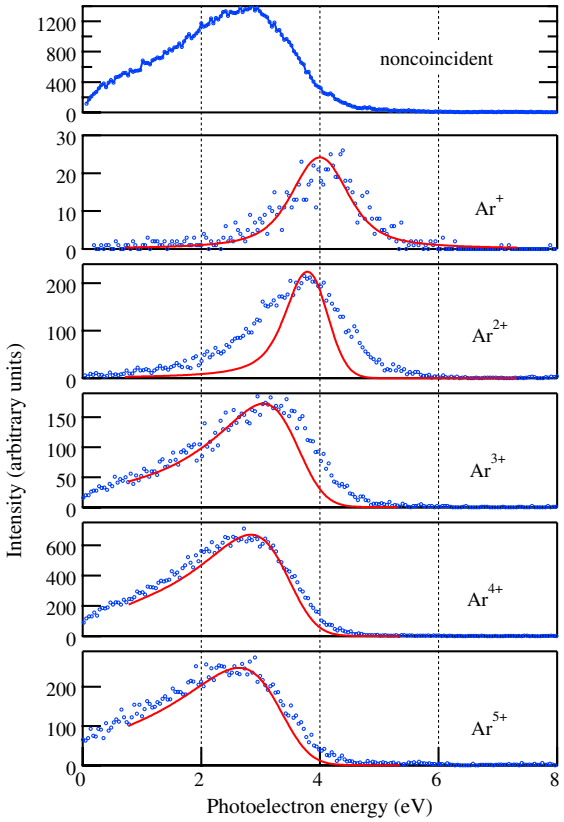

FIG. 3 (color online). Experimental (circles) and theoretical (solid) partial photoelectron spectra measured in coincidence with Ar^{n+} ions ($n = 1$–5) for excess energy 4 eV above IP. The top curve shows the noncoincident photoelectron spectrum.

4 eV ($h\nu = 3210.3$ eV) above ionization threshold, respectively. The different panels on each figure present the spectra recorded in coincidence with Ar^+, Ar^{2+}, Ar^{3+}, Ar^{4+}, and Ar^{5+} ions. With respect to Ar^+, a shift of the maximum of the energy distribution and a distortion of the symmetrical line shape are evidenced for all higher ionic charges. This distortion of the spectra depends on the charge of the residual ion, $n+$: the larger the charge n, the larger the shift and asymmetry of the line shape. Qualitatively, this effect is easily understandable if one takes into account the large energy of the emitted Auger electrons following the creation of the $1s$ vacancy (hundreds to thousands of eV). They quickly leave the zone of reaction and their interaction with the slow photoelectron is negligible. The main contribution to PCI comes from the interaction of the slow photoelectron with the ion field which varies during the course of the Auger decay. Just after $1s$ photoionization, the photoelectron "feels" the field of Ar^{1+}. After the first Auger decay (in SA), it is affected by the field of Ar^{2+}. In the case of DA, the photoelectron motion after an Auger decay is gradually affected by the field of Ar^{2+}, then Ar^{3+}, etc. Because the photoelectron in the course of leaving the atom feels a stronger Coulomb field, its motion is decelerated and its energy decreased. An estimation of the effect can be obtained from the expression for the shift of the maximum given by the eikonal model of PCI in SA [19] and direct DA [9]: $\Delta\epsilon = \xi\Gamma/2$ where Γ is the width of the inner vacancy and the dimensionless parameter ξ takes into account the energies and kinematics of the escaping particles. Neglecting the interaction between the photoelectron and Auger electrons, this parameter has the form: $\xi = \Delta Z/V_{\rm ph}$ where $V_{\rm ph}$ is the velocity of the photoelectron and ΔZ is the change of the ionic charge (the atomic unit system is used throughout). In the more complicated case of cascade MA decays, the shift also depends on the width of the intermediate ionic states.

Calculation of the PCI-distorted photoelectron spectra associated with Eqs. (2) and (3) can be carried out in the framework of the semiclassical approach valid for slow photoelectrons. This approach for SA and cascade DA has been developed in Refs. [10,20], respectively. According to these models, the PCI influence on the line shape mainly depends on the velocity of the slow photoelectron, and on the width Γ of the initial vacancy. In Eq. (2), one has to take into account that the photoelectron moves in the field of the $1s^{-1}$ vacancy before radiative decay, and in the field of the $2p^{-1}$ vacancy after radiative decay and before

Auger decay. Hence, the effective lifetime τ_{eff} of the one-hole state is $\tau_{\text{eff}} = \tau_{1s} + \tau_{2p}$ and the effective width of the initial state is $\Gamma_{\text{eff}} = \Gamma_{1s}\Gamma_{2p}/(\Gamma_{1s} + \Gamma_{2p})$. Using the values of the $1s$ vacancy $\Gamma_{1s} = 690$ meV [21] and of the $2p$ vacancy $\Gamma_{2p} = 118$ meV [22], we find $\Gamma_{\text{eff}} = 101$ meV ($\tau_{\text{eff}} = 6.6$ fs). In Eq. (3), the width of the initial vacancy was also taken to be $\Gamma_{1s} = 690$ meV ($\tau_{1s} = 1$ fs) [21]. Besides, the cross section of Eq. (3) depends also slightly on the width of the intermediate state [10]. There are several different states of the $Ar^{2+*}(2p^{-1}3p^{-1})$ ion depending on the term of the two-hole state [23]. These states vary in energy and can have different widths. We do not distinguish these states and for an estimation of the intermediate state width we use the value $\Gamma_{2p} = 118$ meV ($\tau_{2p} = 5.6$ fs) [22]. In the following, we will associate this effective width with the decay rate weighted average lifetime (DRWAL) which is the averaged characteristic lifetime of the intermediate state involved in each channel of the Auger decay in Eqs. (3)–(5).

Theoretically, the semiclassical approach developed in Ref. [10] can be extended to Eqs. (4) and (5). To our knowledge, the PCI distortion of photoelectron spectra in cascade processes with emission of three or four Auger electrons has never been considered before. We present here, in the framework of a unitary semiclassical approach, the first attempt of a theoretical treatment of PCI induced in the production of highly charged ions. In Eq. (4), we assume direct two-electron emission in the double-Auger decay of $(2p^{-2})$ in the second step of the cascade process. Therefore, we have to modify slightly the parameters C_i in the calculation of the cross section [10]. In Eq. (5), we also used the modified theory from Ref. [10], with the approximation that the Auger decay of the two-hole state $(2s^{-1}2p^{-1})$ occurs by simultaneous emission of three electrons. Using this approach, we need to know the widths of the intermediate states $Ar^{2+*}(2p^{-2})$ and $(2s^{-1}2p^{-1})$. These values can be considered as adjustable parameters in the theory. For the $(2p^{-2})$ state [Eq. (4)], we use the estimated value $\Gamma = 230$ meV (2.8 fs) [21]. The effective width (DRWAL) of the $(2s^{-1}2p^{-1})$ state [Eq. (5)] is fitted to the best agreement with the experimental line shape. Finally, the cross sections of Eqs. (2)–(5) were integrated over all emission angles and convoluted with a Gaussian width of 700 meV to simulate the spectrometer resolution.

A very good agreement is found between the measured and calculated shifts of the maxima of the photoelectron energy distribution as well as for the line shapes for the two photon energies 2 eV (Fig. 2) and 4 eV above threshold (Fig. 3). The ability of our calculations to reproduce the shifts observed at different photon energies, i.e. different photoelectron velocities, reflects the adequacy of our approach. Apart from the velocity of the slow photoelectron, the shift of the line maximum is mainly governed by the width of the initial vacancy. For Eq. (2), the effective value of this width is small, $\Gamma_{\text{eff}} = 101$ meV (6.6 fs), and a small PCI shift is observed compared to Eqs. (3)–(5) where larger shifts are due to the larger value $\Gamma_{1s} = 690$ meV (1 fs). For the cascade processes [Eqs. (3)–(5)], the PCI distortion depends also on the widths of the intermediate states. The good agreement between the measured and calculated shifts and line shapes for Eq. (3) and (4) shows that the values used in our calculation for the DRWAL of the intermediate states $(2p^{-1}3p^{-1})$ and $(2p^{-2})$, 118 meV (5.6 fs), and 230 meV (2.8 fs), respectively, are quite reliable. In Eq. (5), a variation of the values of the effective width of the $(2s^{-1}2p^{-1})$ vacancy in the range 100 to 500 meV leads to a change of the line shift by 0.45 eV. The best agreement with the experimental data is obtained for $\Gamma_{\text{eff}} = 165$ meV (4 fs) and this value can be considered as an estimated value for the $(2s^{-1}2p^{-1})$ vacancy in our model.

Only the main decay pathways are considered in our theoretical calculations. Other pathways may contribute to the formation of each ionic state. For instance, small contributions (4%) from *KMM* decay to the production of Ar^{2+}, and from *LMM* decay (3.3%) to the production of Ar^{3+} were previously documented [15]. These minor contributions will affect the Coulomb field felt by the photoelectron, and distort the measured line shapes. Shake-off electrons with continuous energy sharing may affect the peak shape but not the maximum position. Discrete Auger lines in the kinetic energy range of the photoelectron peak are, however, indistinguishable within our energy resolution and may contribute to the discrepancy between theory and experiment. We can therefore attribute the larger discrepancy observed in the case of Ar^{2+} to various omitted decay channels such as *KMM* decay, *KV* radiative decay followed by autoionization of the valence excited state, or *M* electron shake-off, although these decay channels are not well identified at this point. Uncertainty in the energy of the incoming photons (0.5 eV resolution) may also affect the results. Nevertheless, the general agreement shows the method used allows us to analyze reliably the PCI distortion of the photoelectron spectra, and ascribe the creation of the Ar^{n+} ions to selected MA decay pathways.

In conclusion, Ar $1s$ photoelectron spectra associated with the different ionic states created after core excitation were investigated by electron-ion coincidences. Both measurements and calculation reveal a strong PCI distortion of the photoelectron line. Theoretical analysis allows us to clarify the complicated dynamics of the deep vacancy Auger decay and to estimate the decay rate weighted-average lifetime of the two-hole intermediate states involved in the cascade Auger decay. In comparison with earlier reports, our experimental and theoretical approach is novel as it gives a unique access to the effects of femtosecond lifetimes on the PCI profiles. The comparison between experiment and theory allows us to quantitatively determine poorly known lifetimes, which would be hard or even impossible to determine otherwise.

*Permanent address: Department of Physics and Astronomy, Uppsala University, PO Box 516, SE-751 20 Uppsala, Sweden.

[1] M. N. Piancastelli, J. Electron Spectrosc. Relat. Phenom. **107**, 1 (2000).
[2] M. Yu. Kuchiev and S. A. Sheinerman, Sov. Phys. Usp. **32**, 569 (1989).
[3] V. Schmidt, Rep. Prog. Phys. **55**, 1483 (1992).
[4] F. Penent, J. Palaudoux, P. Lablanquie,L. Andric, R. Feifel, and J. H. D. Eland, Phys. Rev. Lett. **95**, 083002 (2005).
[5] J. H. D. Eland, Adv. Chem. Phys. **141**, 103 (2009).
[6] S. Sheinerman, P. Lablanquie, F. Penent, Y. Hikosaka, T. Kaneyasu, E. Shigemasa, and K. Ito, J. Phys. B **43**, 115001 (2010).
[7] F. Koike, Phys. Lett. A **193**, 173 (1994).
[8] S. A. Sheinerman, J. Phys. B **27**, L571 (1994).
[9] S. A. Sheinerman, J. Phys. B **31**, L361 (1998).
[10] L. Gerchikov and S. Sheinerman, Phys. Rev. A **84**, 022503 (2011).
[11] T. Hayaishi, E. Murakami, Y. Morioka, E. Shigemasa, A. Yagishita, and F. Koike, J. Phys. B **27**, L115 (1994).
[12] G. B. Armen, E. P. Kanter, B. Krässig, J. C. Levin, S. H. Southworth, and L. Young, Phys. Rev. A **69**, 062710 (2004).
[13] A.-M. Flank *et al.*, Nucl. Instrum. Methods Phys. Res., Sect. B **246**, 269 (2006).
[14] K. Ueda, E. Shigemasa, Y. Sato, A. Yagishita, M. Ukai, H. Maezawa, T. Hayaishi, and T. Sasaki, J. Phys. B **24**, 605 (1991).
[15] R. Guillemin, C. Bomme, T. Marin, L. Journel, T. Marchenko, R. K. Kushawaha, N. Trcera, M. N. Piancastelli, and M. Simon, Phys. Rev. A **84**, 063425 (2011).
[16] O. Jagutzki, V. Mergel, K. Ullmann-Pfleger, L. Spielberger, U. Spillmann, R. Dörner, and H. Schmidt-Böcking, Nucl. Instrum. Methods Phys. Res., Sect. A **477**, 244 (2002).
[17] A. G. Kochur, V. I. Sukhorukov, A. I. Didenko, and Ph. V. Demekhin, J. Phys. B **28**, 387 (1995).
[18] U. Alkemper, J. Doppelfeld, and F. von Busch, Phys. Rev. A **56**, 2741 (1997).
[19] M. Yu. Kuchiev and S. A. Sheinerman, Sov. Phys. JETP **63**, 986 (1986).
[20] P. van der Straten, R. Morgenstern, and A. Niehaus, Z. Phys. D **8**, 35 (1988).
[21] M. O. Krause, J. Phys. Chem. Ref. Data **8**, 307 (1979).
[22] M. Jurvansuu, A. Kivimäki, and S. Aksela, Phys. Rev. A **64**, 012502 (2001).
[23] P. Lablanquie, S.-M. Huttula, M. Huttula, L. Andric, J. Palaudoux, J. H. D. Eland, Y. Hikosaka, E. Shigemasa, K. Ito, and F. Penent, Phys. Chem. Chem. Phys. **13**, 18355 (2011).